Gas physisorption studied with density functional theory: application to hysteresis and the Kelvin equation

Onno L.J. Gijzeman[a] and René van Roij[b]

[a] Department of Inorganic Chemistry and Catalysis, Debye Institute, Utrecht University, P.O. Box 80083, 3508 TB, Utrecht, The Netherlands

[b] Institute for Theoretical Physics, Utrecht University, Leuvenlaan 4, 3584 CE, Utrecht, The Netherlands

April 21, 2005

We study nitrogen adsorption on oxidic surfaces within the framework of density functional theory. On the basis of a simple free energy functional, with which we calculate nitrogen density profiles and adsorption isotherms, we argue that some experimental hysteresis effects can directly be related to metastable phases: the jumps in the adsorption occur at the spinodal of the metastable branches. For sufficiently large slits or cylinders this occurs at a "universal" relative pressure of 0.42 in the desorption branch. The agreement of the classical Kelvin theory, used to describe hysteresis by the effect of curved menisci, with our present approach is shown to be approximate only.

1 Introduction

Physisorption of a gas onto a porous substrate has been studied experimentally for more than a century now. An important quantity that is measured is the excess adsorption (per unit area of the substrate) as a function of the relative pressure $p_{rel} = p/p_0$ of the bulk gas in contact with the substrate, at a fixed temperature T. Here p is the actual bulk gas pressure, and $p_0 = p_0(T)$ is the T-dependent saturation pressure, at which the bulk gas coexists with a bulk liquid phase of the adsorbate. The measured adsorption isotherms show a rather diverse behavior, depending on the adsorption strength of the substrate and the interactions between the gas particles [1]. Several classes of been identified and classified according to the IUPAC convention [2]. A very common feature, however, is hysteresis, whereby the adsorbed amount

upon increasing p_{rel} from a low to a high value (the adsorption or gaseous branch) is different from that upon lowering p_{rel} from a high to a low value (the desorption or liquid-like branch). In general both branches of the isotherm are found to show a more or less sharp transition from one to the other at the end points of the hysteresis loop. These transitions are associated with pore filling (or capillary condensation) and pore emtying (or capillary evaporation), respectively. The mechanism underneath the hysteresis effect has been attributed to various origins [3]. One is the presence of a different contact angle of the (supposedly) liquid phase in the pore in going from adsorption to desorption. Also the possibility of the formation of meta-stable phases and pore blocking [4] has been considered. The most common explanation for the effect, however, is the (in)stability of the liquid meniscus at the edge of the pore as described by the classical Kelvin law that relates the pressure difference across a curved interface to the surface tension and the (mean) curvature of the interface. A correction to this law can be added, which accounts for the fact that a pore will have a finite amount of adsorbed molecules with a certain layer thickness, which makes the actual (effective) pore size somewhat smaller than the physical pore size. This approach may not be used for small pores, where the diameter becomes of the order of several adsorbate molecules, and other theories have been proposed to deal with this situation, such as that in Ref. [5] and density functional theory. In the description of hysteresis using Kelvin's law the hysteresis loops are considered to be stable states, corresponding to a thermodynamic equilibrium of a curved liquid-gas interface. The assumption of metastable states does, of course, not consider the branches to be in thermodynamic equilibrium, except at one particular relative pressure.

In this paper we use density functional theory (DFT) [6] to study the adsorption of nitrogen in a single pore, and compare our results with the (macroscopic) Kelvin equation. The focus is on the shift of capilary condensation and evaporation with pore size, and on hysteresis. We do *not* consider freezing in porous materials, and its relation to the (macroscopic) Gibbs-Thomson equation (the crystallization analogue of the Kelvin equation). Studies of capillary freezing were performed recently [7]. Other aspects that we ignore are the effects of a pore size distribution and of connectivity of pores. These effects were addressed recently within a mean-field density functional theory of a disordered lattice gas model [8], and by grand canonical Monte Carlo simulations [9, 10]. Rather we focus on the simpler problem of adsorption of a simple fluid in a planar or cylindrical pore of infinite extension. The DFT approach precludes the effect of a liquid meniscus that may be formed at the ends of or inside the pore. Formation of a meniscus within the fluid was recently treated in Refs.[11, 12], with an emphasis on the behaviour in small pores where the system behaves almost as a one-dimensional confined phase.

DFT is a powerful theoretical framework with which the thermodynamics and structure of fluids in external fields (due to e.g. substrate or a porous medium) can be studied, see e.g. [13, 14, 15, 16, 17, 4, 18]. It is based on the grand-potential functional, which is minimized by the equilibrium density distribution in a given external potential. In the case of adsorption in a pore, be it slit-like or cylindrical, DFT predicts that the excess adsorption can jump, in

thermodynamic equilibrium, to a higher value upon increasing the imposed chemical potential or the external gas density. It is also possible, however, to consider local, but non-global minima of the grand-potential functional, which one associates with metastable states. In this article we not only consider the global, but also other local minima of the functional, and study the stability limits of the (meta)stable branches of the adsorption and desorption isotherms. Some aspects of experimental hysteresis effects can be identified with these limits, and indicate, hence, that the source of the hysteresis loops is the metastability of the states of the adsorbed fluid, at least in some cases.

2 Theoretical

Simple fluids in confining geometries have often been described within the framework of density functional theory. This framework is based on the grand potential density functional [6]

$$\Omega_V[\rho] = \mathcal{F}[\rho] + \int d\mathbf{r}\rho(\mathbf{r})(V(\mathbf{r}) - \mu), \tag{1}$$

where $\mathcal{F}[\rho]$ is the intrinsic free energy functional, $\rho(\mathbf{r})$ the (variational) density of the fluid at position $\mathbf{r}$, $V(\mathbf{r})$ the external (substrate) potential acting on the fluid, and μ the chemical potential as imposed by e.g. a reservoir in contact with the confined geometry. The equilibrium grand potential Ω of the fluid is given, for fixed μ, T, and $V(\mathbf{r})$, by the minimum value of Ω_V, and the minimizing $\rho(\mathbf{r})$ is the equilibrium density profile [6]. Here T is the temperature; for later reference we define $\beta = 1/kT$ with k the Boltzmann constant. In order for the density functional formalism to be of any practical use an explicit form for $\mathcal{F}[\rho]$ is required. This is achieved here by first assuming particle-particle interactions to be of the Lennard-Jones form, with well-depth ϵ_{pp} and "diameter" σ_{pp}, and then to decompose this potential through the Weeks-Chandler-Anderson procedure [19] into a hard-sphere contribution (with a temperature dependent hard-sphere diameter σ) and an attractive long-ranged contribution $\phi_a(r)$ for $r > \sigma$. With this decomposition the intrinsic functional can, within a van der Waals-like mean-field approximation, be written as

$$\mathcal{F}[\rho] = \mathcal{F}_{HS}[\rho] + \frac{1}{2}\int d\mathbf{r}\int d\mathbf{r}'\rho(\mathbf{r})\rho(\mathbf{r}')\phi_a(|\mathbf{r}-\mathbf{r}'|), \tag{2}$$

where $\mathcal{F}_{HS}$ is the hard-sphere functional. Here we consider the form put forward by Tarazona [20]

$$\beta\mathcal{F}_{HS}[\rho] = \int d\mathbf{r}\rho(\mathbf{r})\Big(\ln\rho(\mathbf{r})\Lambda^3 - 1 + \psi(\bar{\rho}(\mathbf{r}))\Big), \tag{3}$$

with Λ the thermal wavelength, $\psi(\rho) = (4\eta - 3\eta^2)/(1-\eta)^2$ the Carnahan-Starling expression for the hard-sphere excess free energy per particle, at packing fraction $\eta = (\pi/6)\sigma^3\rho$, and with

the smooth or weighted density

$$\bar{\rho}(\mathbf{r}) = \int d\mathbf{r}' w(|\mathbf{r}-\mathbf{r}'|;\bar{\rho}(\mathbf{r}))\rho(\mathbf{r}'). \tag{4}$$

Tarazona constructs the weight function $w(r;\rho)$ such that the Percus-Yevick direct correlation function is obtained from the second functional derivative of the excess (over ideal) part of $\mathcal{F}_{HS}[\rho]$. This is achieved by expanding $w(r;\rho) = w_0(r) + \rho w_1(r) + \rho^2 w_2(r)$, with suitably chosen functions $w_i(r)$, see Ref.[20, 18]. Note that erroneous forms for $w_i(r)$ appeared in Ref.[20] *and* its erratum; we used the correct ones given explicitly in the appendix of Ref.[18]. In terms of the auxilary smooth densities $\bar{\rho}_i(\mathbf{r}) = \int d\mathbf{r}' w_i(|\mathbf{r}-\mathbf{r}'|)\rho(\mathbf{r}')$, for $i = 0, 1, 2$, the weighted density is easily found as the (physical) solution of the quadratic equation $\bar{\rho}(\mathbf{r}) = \bar{\rho}_0(\mathbf{r}) + \bar{\rho}_1(\mathbf{r})\bar{\rho}(\mathbf{r}) + \bar{\rho}_2(\mathbf{r})\bar{\rho}(\mathbf{r})^2$ [20]. From this the minimum condition for $\Omega_V[\rho]$, $\delta\Omega_V/\delta\rho(\mathbf{r}) = 0$, can be written as

$$\begin{aligned} \beta\mu &= \ln\rho(\mathbf{r})\Lambda^3 + \psi(\bar{\rho}(\mathbf{r})) + \int d\mathbf{r}'\rho(\mathbf{r}')\psi'(\bar{\rho}(\mathbf{r}))\frac{w(|\mathbf{r}'-\mathbf{r}|;\bar{\rho}(\mathbf{r}))}{1-\bar{\rho}_1(\mathbf{r}')-2\bar{\rho}_2(\mathbf{r}')\bar{\rho}(\mathbf{r}')} \\ &+ \int d\mathbf{r}'\rho(\mathbf{r}')\beta\phi_a(|\mathbf{r}'-\mathbf{r}|) + \beta V(\mathbf{r}). \end{aligned} \tag{5}$$

This nonlinear integral equation for the equilibrium density $\rho(\mathbf{r})$ can be solved iteratively on a spatial grid.

In the present paper we are interested in external potentials in the pores of a porous medium. This medium, which forms the walls of the pore, is assumed to be inert, homogeneous and of bulk number density ρ_w. Assuming a pair potential $\varphi(r)$ between the adsorbed fluid particles and the particles of the medium, one can write the external potential as

$$V(\mathbf{r}) = \rho_w \int_{\text{medium}} d\mathbf{r}'\varphi(|\mathbf{r}'-\mathbf{r}|), \tag{6}$$

where the integration is over that part of the volume that is occupied by the inert medium, i.e. one assumes a step function for the density of the medium. In our model calculations we assume that the adsorbing surfaces, i.e. the boundaries between the pore and the medium, are molecularly smooth and infinitely extended. We restrict attention to two cases: (i) the planar slit of width H in between two half-spaces $z < 0$ and $z > H$ of the medium, where z is the cartesian coordinate parallel to the surface normal of the medium, and (ii) the cylindrical slit of diameter D, with a radial coordinate R in the range $0 < R < D/2$. As a result the pores have a symmetry such that $V(\mathbf{r}) = V(z)$ in the planar geometry, and $V(\mathbf{r}) = V(R)$ in the cylindrical geometry. We now assume that $\varphi(r)$ is of the Lennard-Jones form, with well depth ϵ_{pw} and "diameter" σ_{pw}. For the planar slit one then obtains $V(z) = V_1(z) + V_1(H-z)$, where the external potential due to the half space $z < 0$ follows from Eq.(6) as

$$V_1(z) = 4\pi\epsilon_{pw}\rho_w\sigma_{pw}^3\left(\frac{1}{45}\frac{\sigma_{pw}^9}{z^9} - \frac{1}{6}\frac{\sigma_{pw}^3}{z^3}\right). \tag{7}$$

Note that depth of $V_1(z)$ is characterised completely by the parameter combinations $\epsilon_{pw}\rho_w\sigma_{pw}^3$, where we expect $\rho_w\sigma_{pw}^3$ to be of order unity. The external potential in the cylinder geometry is given, for $0 \leq R \leq D/2$, by

$$V(R) \;=\; \rho_w \int_{-\infty}^{\infty} dz' \int_{D/2}^{\infty} dR' R' \int_0^{2\pi} d\phi' \varphi(\sqrt{R^2 + R'^2 - 2RR'\cos\phi' + z'^2}), \tag{8}$$

where the z' integration can readily be done analytically. The remaining double integration over R' and ϕ' was performed numerically once, for a given D, and stored.
In order to reduce the computational cost of solving Eq.(5), we now assume that the equilibrium density profile $\rho(\mathbf{r})$ is of the same symmetry as the external potential in the pore, i.e. $\rho(\mathbf{r}) = \rho(z)$ in the planar slit and $\rho(\mathbf{r}) = \rho(R)$ in the cylindrical slit. This assumption, in which possible symmetry-breaking phenomena such as capillary crystallisation are ignored, allows for a simple one-dimensional spatial grid onto which Eq.(5) can be solved. In order to evaluate the expressions of the form $\int d\mathbf{r}' k(|\mathbf{r} - \mathbf{r}'|)\rho(\mathbf{r}')$, with $k(r) = w_i(r)$ or $k(r) = \phi_a(r)$, one must yet perform the integrations over the remaining coordinates, i.e. over the transversal coordinates x and y in the planar geometry and over the coordinates z and ϕ in the cylinder geometry. These integrals then take the form $\int dz' K(|z-z'|)\rho(z')$ (planar) or $\int dR' K(R, R')\rho(R')$ (cylinder). The resulting integrated kernels K need, however, be calculated only once, either numerically or analytically. Once the equilibrium distributions $\rho(z)$ or $\rho(R)$ have been found, the dimensionless excess adsorption (per unit area) follows as

$$\Gamma = \begin{cases} \sigma^2 \displaystyle\int_0^{H/2} dz\Big(\rho(z) - \rho_b\Big) & \text{(planar slit)} \\ \dfrac{2\sigma^2}{D} \displaystyle\int_0^{D/2} dRR\Big(\rho(R) - \rho_b\Big) & \text{(cylinder),} \end{cases} \tag{9}$$

where H is the wall-wall distance of the planar slit, and D the diameter of the cylindrical slit. Here ρ_b is the density of a bulk fluid at the chemical potential μ and temperature T.
We will present our results in terms of the pressure $p = p(\mu, T)$ of a bulk fluid at temperature T and chemical potential μ. This pressure equals the negative of the equilibrium grand potential per unit volume of the homogeneous bulk fluid.

3 Results

3.1 Choice of parameters

The adsorbate of interest here is nitrogen, N_2, at its standard (1 atmosphere) boiling temperature $T = 77$K, and the adsorbing medium is an oxidic surface. Our task is now to find explicit numerical values for the nitrogen parameters ϵ_{pp} and σ (and hence σ_{pp}), and for the

nitrogen-wall parameters $\epsilon_{pw}\rho_w\sigma_{pw}^3$, and σ_{pw}. A relatively simple way to get values for the nitrogen parameters would be to fit some properties of the bulk phase diagram to experimentally known quantities. One could, for instance, match the theoretical bulk critical point parameters $(\beta\epsilon_{pp}, \rho\sigma^3)_{crit} = (1.03, 0.249)$ to the experimental critical temperature $T_c = 126.3$K and critical density $\rho_c = 6.6815\text{nm}^{-3}$ to obtain $\beta\epsilon_{pp} = 1.69$ and $\sigma = 3.34$Å. [Note that the critical value of $\beta\epsilon_{pp}$ that follows from the WCA procedure differs substantially from the value one would obtain if the hard-core diameter were independent of the temperature.] Similar, but not identical, numbers are obtained when other combinations of critical constants are taken, e.g. the critical pressure p_c and T_c, or p_c and ρ_c. However, since the temperature of interest is far below T_c (the experimental numbers give $T/T_c = 0.61$), we argue that fitting to the critical constants is not optimal. We decided, as an alternative, to fit the theoretically obtained adsorption isotherm of a single planar wall, i.e. with $V(z) = V_1(z)$, to the classical de Boer $T = 77$K isotherm for the adsorption of nitrogen on oxidic surfaces [21]. This experimental isotherm is e.g. tabulated by Adamson [1]. The fit, which is shown in Fig.1, yields $\beta\epsilon_{pp} = 1.72$, $\epsilon_{pw}\rho_w\sigma_{pw}^3 = 7.5\epsilon_{pp}$, $\sigma = 4.52$Å, and $\sigma_{pw}/\sigma = 0.8$. Here the value for σ was obtained by simple scaling, i.e. by connecting the excess adsorption in units of σ^3 and the actual amount, given by de Boer, in cm^3. The other three fit parameters follow from the best fit to the shape of the adsorption isotherm. Clearly the resulting value for σ deviates considerably from the one obtained from a fit to the critical constants. The fit to the de Boer data compares, however, favourably with the ratio T/T_c, which is now predicted to be 0.60 compared to the experimental value 0.61. Also the resulting prediction for the density ρ_g of the saturated gas, $\rho_g\sigma^3 = 0.00993$, is in reasonable agreement with the experimental value, which with the fitted value of $\sigma = 4.52$Å gives $\rho_g\sigma^3 = 0.00866$. The isosteric heat of adsorption that we obtain from these model parameters is in agreement with experiment: it increases with coverage up to about the first monolayer, then shows a sharp drop, and it approaches, but never reaches, the value of the heat of condensation for a bulk liquid [22]. By decreasing the wall-particle interaction strength, we also checked that the model reproduces the various shapes of physisorption isotherms, e.g. a more gradual increase in the amount adsorbed with pressure was thus obtained.

All in all the present theory, fitted to the de Boer isotherm, seems to account satisfactorily for the adsorption of nitrogen on oxidic surfaces. It is less elaborate than other (similar) approaches, where e.g. the radial distribution function of the hard-sphere fluid is required as input [13], or where the external potential is more complicated [14, 15, 17]. Of course the fit parameters could be adjusted to other quantities, and different numbers would be obtained. The present values are, however, acceptable for our purposes, as they do not influence our results on hysteresis, to be discussed further on.

3.2 Pores

Now that we have found the parameters that reasonably reproduce experimental results for adsorption on a flat surface, it is of interest to extend the calculations to adsorption and desorption in slits and cylinders. These calculations were done by computing, from Eq.(5), the density profiles for the adsorption branch with increasing relative pressures, using the previous (lower pressure) profile as a starting point for the next profile. For the computation of the desorption branch the starting point for the profile to be found was that of the previous (higher) pressure profile. Fig.2 shows the resulting isotherms for cylinders of several diameters D. The data for planar slits look similar. For $D \geq 6$ we distinguish a low-Γ ("gaseous") and a high-Γ ("liquid-like") branches, and jumps between them which feature hysteresis: the jump of the desorption and adsorption curves do not coincide. Hysteresis is also a common experimental fact in large enough pores. The grand potential of the two profiles at a given relative pressure differ in general, and the profile with the lowest grand potential corresponds to the stable thermodynamic state, the other one is metastable. The equilibrium jump in the adsorption takes place at that relative pressure where the grand potential of the two branches are equal. This is illustrated in Fig.3, where the excess adsorption and the grand potential Ω are shown as a function of the relative pressure, for $D = 24\sigma$. Fig.3 shows that the thermodynamic equilibrium jump, i.e. the equilibrium capillary condensation, takes place at $p/p_0 \simeq 0.60$, which is in between the two endpoints of the hysteresis loop at $p/p_0 \simeq 0.38$ and 0.66. The computed endpoints of the hysteresis loop turn out to be caused by an intrinsic (spinodal) instability in the system, and *not* by the specific computational procedure we used. This is illustrated in Figs.4 and 5, where we zoom into those parts of the adsorption isotherm of $D = 6\sigma$ where the hysteresis jumps of the adsorption (Fig.4) and desorption (Fig.5) branch take place. The diverging slope of both curves indicates that $d\Gamma/d\mu$ diverges, i.e. that a (surface) spinodal point is approached. The same effect was found for all cylindrical and planar slits that we investigated numerically. A similar conclusion was obtained from canonical Monte Carlo simulations in Ref.[23]. Comparing those results with experiments the authors of Ref.[23] found that for sufficiently large pores (larger than 14σ) capillary condensation occurs at the surface spinodal of the adsorption branch, whereas the capillary evaporation upon desorption occured at the point of the equilibrium transition. We remark here, however, that experiments on different systems [24, 25, 26] indicate that the jump in the desorption branch for pores larger than about 30σ takes place at a fixed, universal relative pressure of about 0.42. This effect will be discussed further on.

The data of Fig.2, as well as its planar slit analogue, show that the hysteresis loop decreases with decreasing pore size in two senses. On the one hand the endpoints of the hysteresis loop (the values of p/p_0) approach each other, and on the other the jump of Γ decreases. Closer inspection shows that the equilibrium adsorption jump, called $\Delta\Gamma$ from now on, has an interesting structure for small planar slits. This is illustrated in Fig.6, where $\Delta\Gamma$ is shown as a

function of the slit width H. For large slit widths the curve is smooth and does not feature any discontinuities (or they are so small that we cannot discern them), and extrapolation of the large-H part of the curve to the small-H regime seems to yield a well-defined critical separation H_c where $\Delta\Gamma = 0$. This value for H_c would corresponds to the capillary critical point at the current temperature, which separates the high-H regime of a first-order capillary condensation and the low-H regime of continuous filling of the slit. However, the numerical data for $\Delta\Gamma$ at $H < 4.5\sigma$ shows levels of constant $\Delta\Gamma$ separated by discontinuities. The same was found for cylindrical pores. We traced these levels back to packing effects, which cause the maximum amount adsorbed in a slit (or cylinder) to be a discontinuous function of its size, as noted by many authors [13]. On the basis of universality of critical phenomena, we do not expect, however, that $\Delta\Gamma$ exhibits a jump from a finite value to zero, but instead approaches zero continuously with a universal exponent [27]. This behaviour should take place in a very narrow slit width interval $4 < H/\sigma < 4.1$, that we did not investigate in more detail since the values of $\Delta\Gamma$ become extremely small. For all practical purposes one can state that the hysteresis effect disappears completely for planar slits for which $H < 4\sigma$. For cylinders it is found to disappear if $D < 4\sigma$.

The disappearance of hysteresis for small enough pores is also found experimentally, e.g. in MCM materials [28, 29, 30, 31]. This is a class of highly uniform mesoporous (alumino)silicates, consisting only of cylindrical pores of fixed diameter, without any appreciable external surface area. An example of our experimental adsorption and desorption curves of such a material is shown in Fig.7. It shows virtually perfect overlap, i.e. no hysteresis, in agreement with the theory.

3.3 The origin of hysteresis

We have seen that the theory predicts that adsorption-desorption hysteresis can occur in sufficiently large pores (both cylindrical and planar), and that this hysteresis effect disappears, for all practical purposes, when the diameter is less than about 4σ. Commonly these observed hysteresis loops are attributed to the effect of curvature of the liquid meniscus as described by the (modified) Kelvin equation, which expresses the relative pressure $p_{rel} = p/p_0$ at which pore condensation and pore evaporation take place in the adsorption and desorption process, respectively. Here we compare our density functional calculations with those based on the Kelvin equation.

The Kelvin equation relates the pressure difference accross an interface to the curvature and surface tension of that interface. For the adsorption branch of cylinders, the Kelvin equation is often written as [3, 32]

$$\ln p_{rel} = -\frac{2\gamma}{kT\rho_l}\frac{1}{D/2 - t}, \tag{10}$$

and for the desorption branch as

$$\ln p_{rel} = -\frac{2\gamma}{kT\rho_l}\frac{2}{D/2-t}. \tag{11}$$

The factor of two in the difference between the Kelvin equation for the adsorption and desorption branch is caused by the presence of a spherical hemisphere of liquid at the edge of the cylinder in the latter case. In the Eqs.(10) and (11) γ is the bulk gas-liquid surface tension (at the temperature under consideration), ρ_l is the coexisting bulk liquid density (which is assumed to be much higher than the saturated gas density), and t is the mean thickness of the liquid layer adsorbed onto the wall of the cylindrical pore. This layer reduces the effective radius of the cylinder from its bare value, $D/2$, to $D/2-t$. The mean thickness is calculated from an (empirical) relation for the adsorption isotherm on a flat surface, which is in fact nothing but a parametrisation of the data in Fig.1 for the prevailing relative pressure. The resulting thickness, t_{flat}, of the adsorbed layer on the flat surface is then converted to the value t in the cylindrical pore by the relation

$$t = \frac{D}{2}\left(1-\sqrt{1-\frac{4t_{flat}}{D}}\right). \tag{12}$$

This conversion is based on the fact that the adsorbed amount in a cylinder and on a flat surface are equal at the same relative pressure. [Note that $t \to t_{flat}$ when $D \to \infty$, as expected.] This conversion is usually not implemented [32], however, the error is small, as will be shown later. Note that the Kelvin approach predicts that hysteresis will take place in the adsorption-desorption branch regardless of the cylinder diameter, whereas it predicts *no* capillary condensation in filling a slit like pore. The Kelvin approach can be criticised on many grounds. For instance, the adsorbed layer is not a bulk liquid, so the value of the surface tension to be used should not be that of the bulk liquid. Also the use of a macroscopic equation to describe a meniscus on a molecular scale may be incorrect. Moreover, the equations (10) and (11) are based on the assumption that the film of adsorbed molecules is homogeneous, whereas intuition, DFT, and even the classical BET theory [33] predict that successively adsorbed layers show a decreasing density in going away from the surface. So the concept of a well-defined adsorbed layer thickness is at best nebulous. Finally, we mention that the underlying mechanism of hysteresis as predicted by the Kelvin equations (10) and (11) is governed by the (lack of) stability of the liquid meniscus at the edge of the cylindrical pore or the planar slit. Given that the pore and the slit are assumed to be infintely extended, this implies that fluctuations inside the cavity are assumed to be irrelevant for the state of the fluid in the cavity —as long as the edge is stable. This seems quite unlikely.

It can, however, also be argued that application of the modified Kelvin equation gives in many cases quite reasonable values for the measured pore diameters. This observation may in fact

be just coincidental. From our DFT data such as those given in Fig.2 we can easily extract those values of the relative pressure where, for a given cylinder diameter or slit width, the jump takes place in adsorption and desorption branch. The resulting relation between the relative pressure (at which the adsorption jump occurs) and the cylinder diameter is shown in Fig.8, together with the results based on the Kelvin equations (10) and (11). For the latter we used the experimental surface tension. The rather small effect of using t_{flat} instead of t in the Kelvin equations is shown by the dashed curves. For the case of adsorption the difference between DFT and Kelvin is within a factor of three for large D. For narrow pores with $D < 5\sigma \simeq 20\text{Å}$ the discrepancy is larger. For desorption branch the agreement between DFT and Klevin appears to be even worse. The comparison between DFT and Kelvin for the case of the planar slit is shown in Fig.9, of course only for the desorption branch. The agreement is as poor as for the desorption curves in cylinders shown in Fig.8, but could be improved by adjusting the the value of σ.

An interesting aspect of our DFT data is, however, that large cylinders and slits, with say $D, H > 30\sigma$, exhibit the jump in the desorption branch independent of the pore size, i.e. they empty at a relative pressure $p/p_0 \simeq 0.42$. This phenomenon, which has often been observed experimentally for the desorption branch [24, 25, 26], is in gross disagreement with the Kelvin equation (11). If one, nevertheless, analyses the pore size distribution of a porous medium on basis of the desorption branch combined with Eq.(11) —as is often done in e.g. software that comes with commercial equipment— one finds a peak at that value of D where the right hand side of Eq.(11) matches $\ln(0.42)$. Of course this peak is an artifact of such an analysis, and various explanations of its origin have been given. It has been argued, for instance, that the capillary stress exceeds the tensile stress of the condenstate [3, 34], or that micropore filling coincides with the locus of capillary evaporation-capillary condensation coexistence in equilibrium [25]. Our results strongly suggest, however, that this effect is caused by the presence of a *bulk* spinodal point —which is of course independent of the pore parameters. This is illustrated in Fig.10, where we show the density profiles of the desorption branch of the planar slit, with $H = 50\sigma$, at several pressures. At the highest pressure, $p/p_0 = 1$, the density strongly oscillates up to the middle of the slit. This persistent oscillation could well an artifact of the employed density functional at our parameter choice. However, at lower relative pressures, say $p/p_0 \leq 0.6$, the profile is essentially flat in the middle of the slit as one might anticipate for a dense homogeneous fluid. This constant density in the middle of the slit is lower than that of the bulk liquid phase at coexistence, and it decreases when the pressure is decreased further. At a certain relative pressure (for our parameter set at $p_{rel} = 0.42$) the liquid bulk spinodal point at the temperature of interest is reached. The corresponding spinodal bulk density ρ_{spin} is given, within the present Van der Waals-Carnahan-Starling theory to which our functional reduces for a bulk fluid, by $\rho_{spin}\sigma^3 = 0.56$. This corresponds precisely to the central density in the slit at $p_{rel} = 0.42$, as shown by the blow-up in the lower-right corner of Fig.10. At lower values of p_{rel} the homogeneous liquid in the middle of the slit is unstable with respect to

infinitesimal density fluctuations, and collapses: the pore empties. This effect is independent of the exact slit size (or cylinder radius) provided that the pore is large enough to develop a constant density in its central region.
We consider the agreement between the DFT calculations and the experimental observation of pore-emptying at $p_{rel} \simeq 0.42$ in large pores [24, 25, 26] as evidence for the fact that the experimentally observed hysteresis is caused by the spinodal rather than by pore-edge effects underlying the Kelvin approach. The difference with the experiments discussed in Ref.[23], where the desorption branch empties at the equilibrium transition, could be due to the effects of fluctuations, which may cause cavitation prior to to mean-field spinodal. This issue deserves further investigation.

4 Summary and conclusions

We have performed density functional calculations of physisorption of nitrogen on oxidic surfaces. We found reasonably good agreement with some experimenal observations, despite the fact that our functional treats the dispersion forces on the Van der Waals-like mean-field level. The theory is able to reproduce adsorption isotherms on flat surfaces using a very limited number of parameters, and it predicts hysteresis effects in pores that are not caused by the effect of curved menisci, but rather by the (spinodal) instability of the adsorbed phases. The occurrence of a lower relative pressure limit in desorption experiments of about 0.42 is predicted correctly. This feature is completely missed by the standard Kelvin approach to estimate the limits of hysteresis. Also the estimate of the pore-size from the hysteresis loop on the basis of the Kelvin equation can differ by factors larger than three from the DFT values, especially if the pores are small. In addition, unlike the Kelvin approach the present theory predicts the (experimentally observed) disappearance of the hysteresis effects for small enough pores. For these reasons the present theory, and the present choice of parameters, could be useful to analyse adsorption phenomena of nitrogen on oxidic surfaces.

5 Acknowledgement

This work is part of the Research program of the "Stichting voor Fundamenteel Onderzoek der Materie (FOM)", which is financially supported by the "Nederlandse Organisatie voor Wetenschappelijk Onderzoek (NWO)".

References

[1] A.W. Adamson and A.P. Gast, *Physical Chemistry of Surfaces*, 6th ed., John Wiley & Sons, Inc. (1997).

[2] K.S.W. Sing, Pure and Appl. Chem. **54**, 2201 (1982).

[3] S.J. Gregg and K.S.W. Sing, *Adsorption, Surface Area and Porosity*, 2nd ed., Academic Press, London, 1982.

[4] P.C. Ball and R. Evans, Langmuir **5**, 714 (1989).

[5] M.M. Dubinin, Chem. Rev. **60**, 235 (1960).

[6] R. Evans, Adv. Phys. **28**, 143 (1979).

[7] R. Radhakrishnan, K.E. Gubbins, M. Sliwinska-Bartkowiak, J.Chem. Phys. **116**,1147 (2002); *ibid.* J. Chem. Phys. **112**, 11048 (2000).

[8] E. Kierlik, P.A. Monson, M.L. Rosinberg, L. Sarkisov, and G. Tarjus, Phys. Rev. Lett. **87**, 055701 (2001).

[9] S. Gavalda, K.E. Gubbins, K. Kaneko, and K.T. Thomson, Langmuir **18**, 2141 (2002).

[10] A. Vishnyakov, P.G. Debenedetti, and A. Neimark, Phys. Rev. E **62**, 538 (2000).

[11] G.S. Heffelfinger, F. van Swol, and K.E. Gubbins, J. Chem. Phys. **89**, 5202 (1988).

[12] B.K. Peterson, K.E. Gubbins, G.S. Heffelfinger, U. Marini Bettolo Marconi, and F. van Swol, J. Chem. Phys. **88**, 6487 (1988).

[13] J.P. Olivier, J. Porous Materials **2**, 9 (1995).

[14] P.I. Ravikovitch, A. Vishnyakov, R. Russo, and A.V. Neimark, Langmuir **16**, 2311 (2000).

[15] C. Lastoskie, K.E. Gubbins, and N. Quirke, Langmuir **9**, 2693 (1993); J. Phys. Chem. **97**, 4786 (1993).

[16] N.A. Seaton, J.P.R.B. Walton, and N. Quirke, Carbon **27**, 853 (1989).

[17] M. El-Merraoui, M. Aoshima, and K. Kaneko, Langmuir **16**, 4300 (2000).

[18] P. Tarazona, U. Marini Bettolo Marconi, and R. Evans, Mol. Phys. **60**, 573 (1987).

[19] J.D. Weeks, D. Chandler, and H.C. Anderson, J. Chem. Phys. **54**, 5237 (1971).

[20] P. Tarazona, Phys. Rev. A **31**, 2672 (1985); Phys. Rev. A **32**, 3148 (1985).

[21] B.C. Lippens, B.G. Linsen, and J.H. de Boer, J. Catal. **3**, 32 (1964); J.H. de Boer, B.C. Lippens, B.G. Linsen, J.C.P. Broekhoff, A. van den Heuvel, and Th. J. Osinga, J. Coll. Interface Sci. **21**, 405 (1956).

[22] L.G. Joyner and P.H. Emmett, J. Amer. Chem. Soc. **70**, 2353 (1948); A. Thomy, and X. Duval, and J. Regnier, Surface Science Rep. **1**, 1, (1981).

[23] P.I. Ravikovitch, A. Vishnyakov, and A. Neimark, Phys. Rev. E **64**, 011602 (2001).

[24] O. Kadlec and M.M. Dubinen, J. Colloid. Interface. Sci. **31**, 479 (1969); C.G.V. Burgess and D.H. Everett, J. Colloid. Interface. Sci. **33**, 611 (1970).

[25] S.K. Bhatia and H.K. Shethna, Langmuir **10**, 3230 (1994).

[26] J.C. Groen, L.A.A. Peffer, and J. Pérez-Ramírez, Micropor. Mesopor. Mater. **51**, 75 (2002).

[27] R. Evans, U. Marini Bettolo Marconi, and P. Tarazona, J. Chem. Phys. **84**, 2376 (1986).

[28] H. Kanda, M. Miyahara, T. Yoshioka, and M. Okazaki, Langmuir **16**, 6622 (2000).

[29] M. Hakuman and H. Naono, J. Colloid. Interface. Sci. **241**, 127 (2001).

[30] J. Goworek, J. Wawryszczuk, and R. Zaleski, J. Colloid. Interface. Sci. **243**, 427 (2001).

[31] M. Kruk and M. Jaroniec, J. Phys. Chem. B **106**, 4732 (2002).

[32] S. Lowell and J.E. Shields, *Powder Surface Area and Porosity*, 2nd ed., Chapman and Hall Ltd., London, (1984).

[33] S. Brunauer, P.H. Emmett, and E. Teller, J. Amer, Chem. Soc. **60**, 309 (1938).

[34] D.H. Everett, in *The gas-solid interface*, E.A. Flood, Ed., Marcel Dekker: New York, 1967.

Fig.1 Adsorption isotherm of nitrogen on a single planar oxidic wall at $T = 77$K as measured by the De Boer and calculated by the present theory (see text).

Fig.2 Adsorption and desorption isotherms of nitrogen in oxidic cylindrical pores with diameters D indicated in units of the nitrogen hard-sphere radius $\sigma = 4.52$Å.

Fig.3 Adsorption and desorption isotherm in cylindrical pore of diameter $D = 24\sigma$ (upper graph), and the corresponding grand potential (lower graph). The vertical dashed lines denote the end-points of the hysterisis loop, and the vertical dot-dashed line the equilibrium transition point.

Fig.4 Blow-up of the adsorption branch of a cylindrical pore of diameter $D = 6\sigma$. The diverging slope of the curve indicates that a surface spinodal point is approached.

Fig.5 As Fig.4, but now the desorption branch.

Fig.6 The equilibrium adsorption jump $\Delta\Gamma$ as a function of the width H of the planar slit. In the regime $4 < H/\sigma < 4.5$ packing effects cause nonmonotonic and discontinuous behaviour.

Fig.7 Experimental adsorption and desorption isotherms (in units of cm^3 STP/g) of nitrogen in MCM (see text), showing *no* hysteresis.

Fig.8 The onset of the jumps in the adsorption and desorption branch for cylinders of various diameters (expressed in units of the nitrogen hard-core diameter σ) as a function of the relative gas pressure. Both the present DFT results (where the jumps coincide with the adsorption spinodal) and those of the modified Kelvin equations (10) and (11) are given. The dashed line represents the result with $t = t_{flat}$ (see text).

Fig.9 As Fig.8, but now for planar slits of various widths, and only the desorption branch.

Fig.10 Density profiles for the adsorption in a slit of width $H = 50\sigma$ at various relative pressure. All plots are on the same scale, except for the bottom right which is an enlargement of the one above. Note the loss of structure in the central region of the slit with decreasing pressure, which leads to the formation of a homogeneous bulk phase that is stabilised by the presence of adsorbed layers near the walls, until its spinodal point is reached at $p_{rel} = 0.42$.

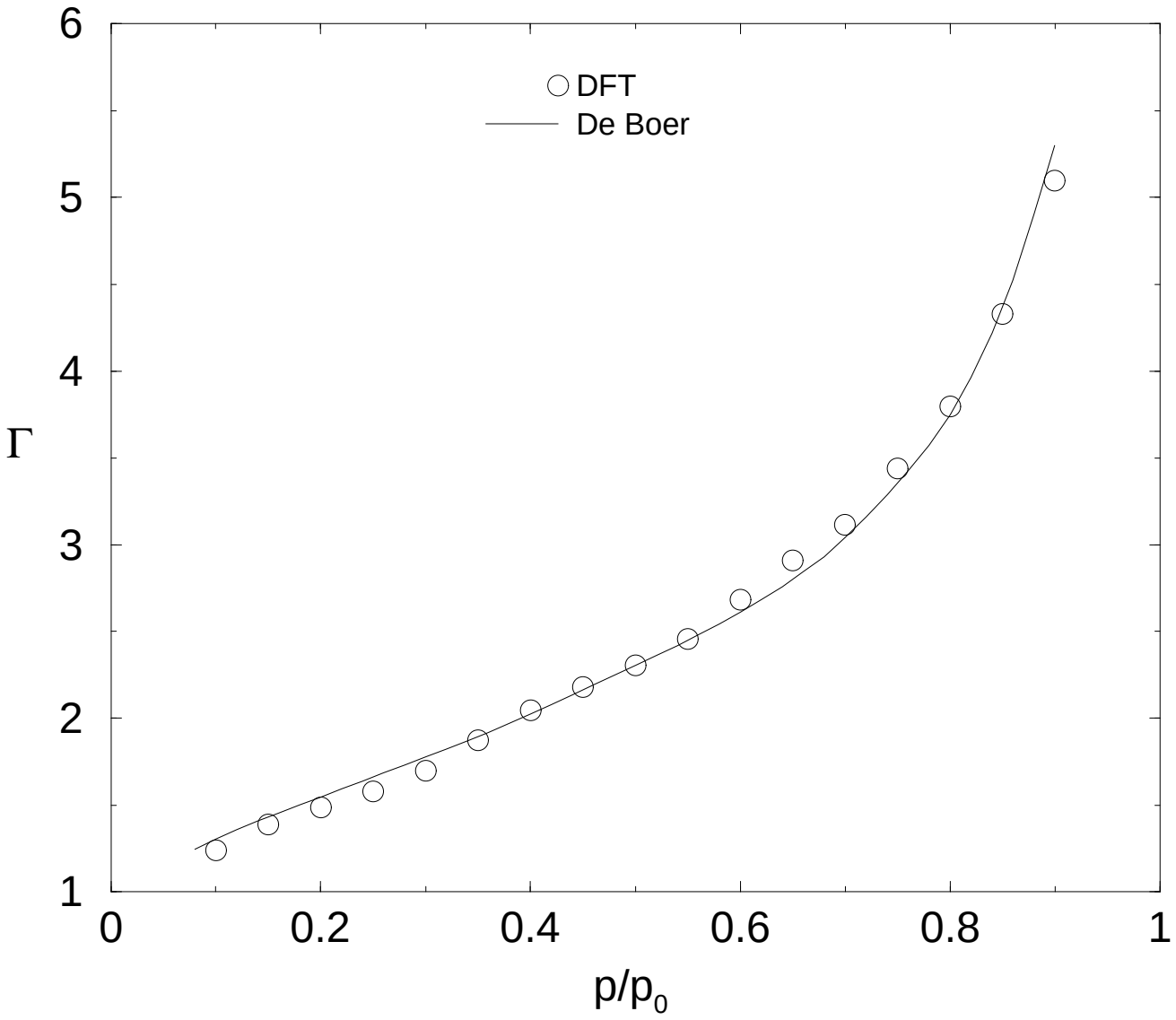

Figure 1: O. Gijzeman and R. van Roij

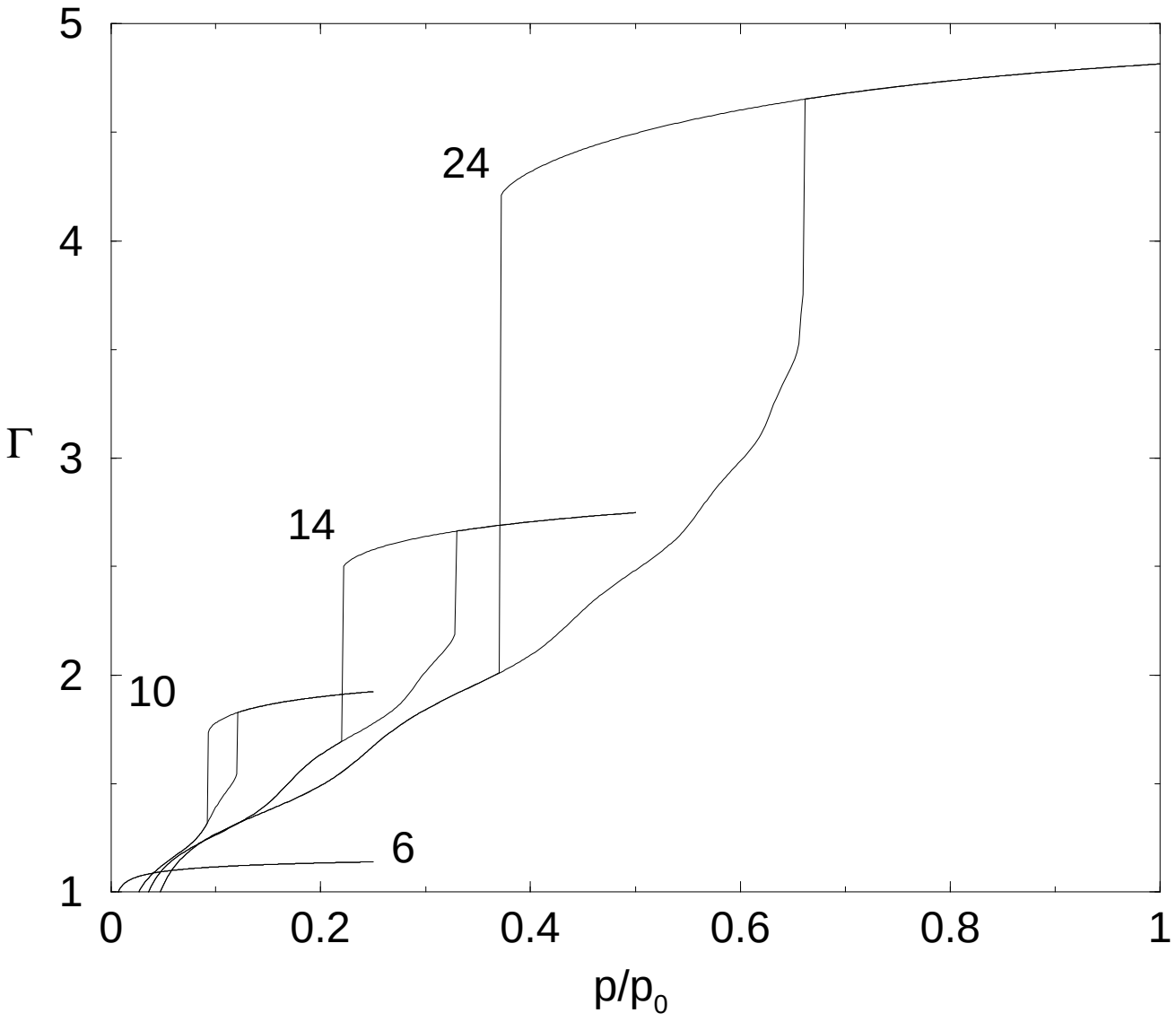

Figure 2: O. Gijzeman and R. van Roij

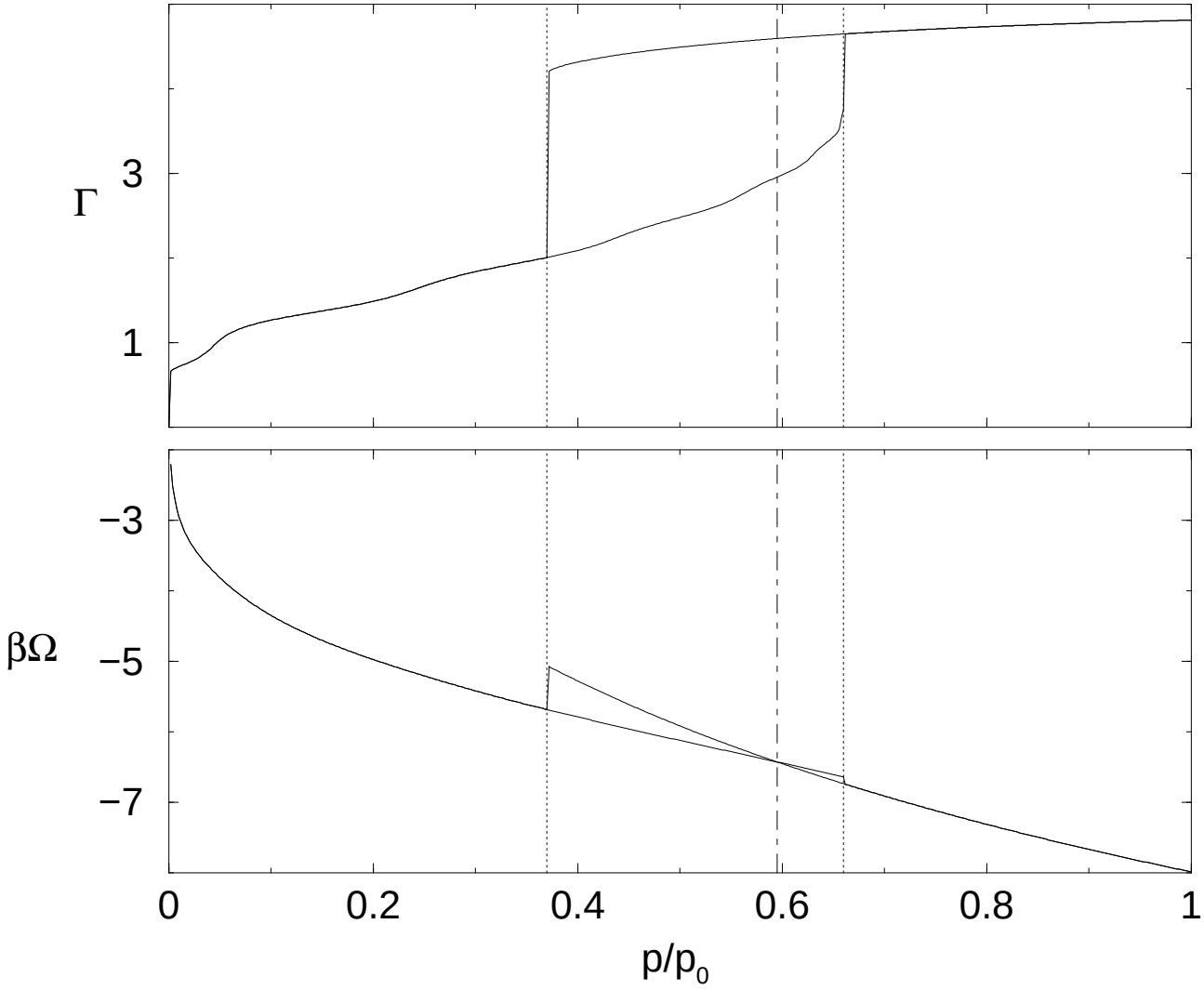

Figure 3: O. Gijzeman and R. van Roij

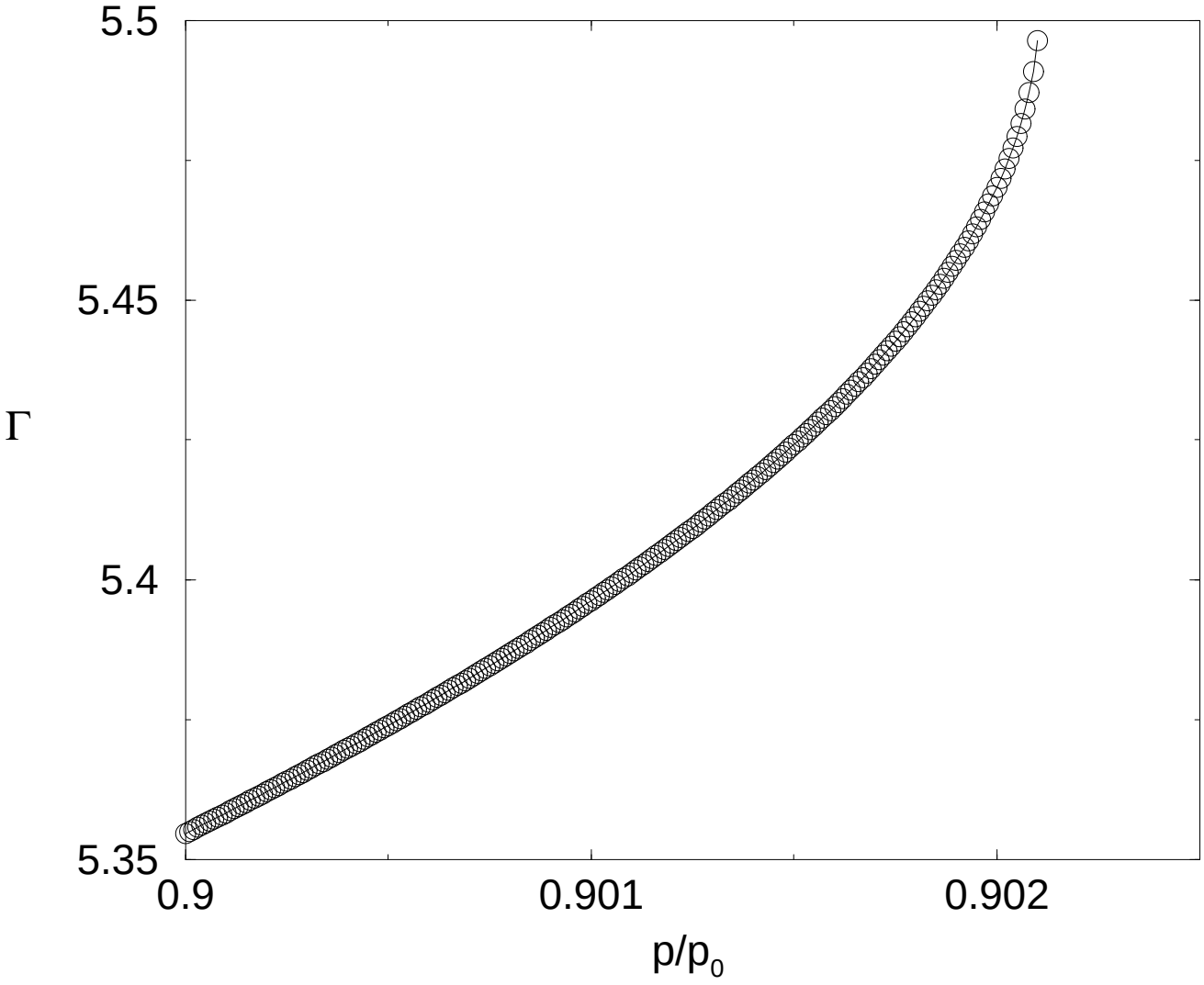

Figure 4: O. Gijzeman and R. van Roij

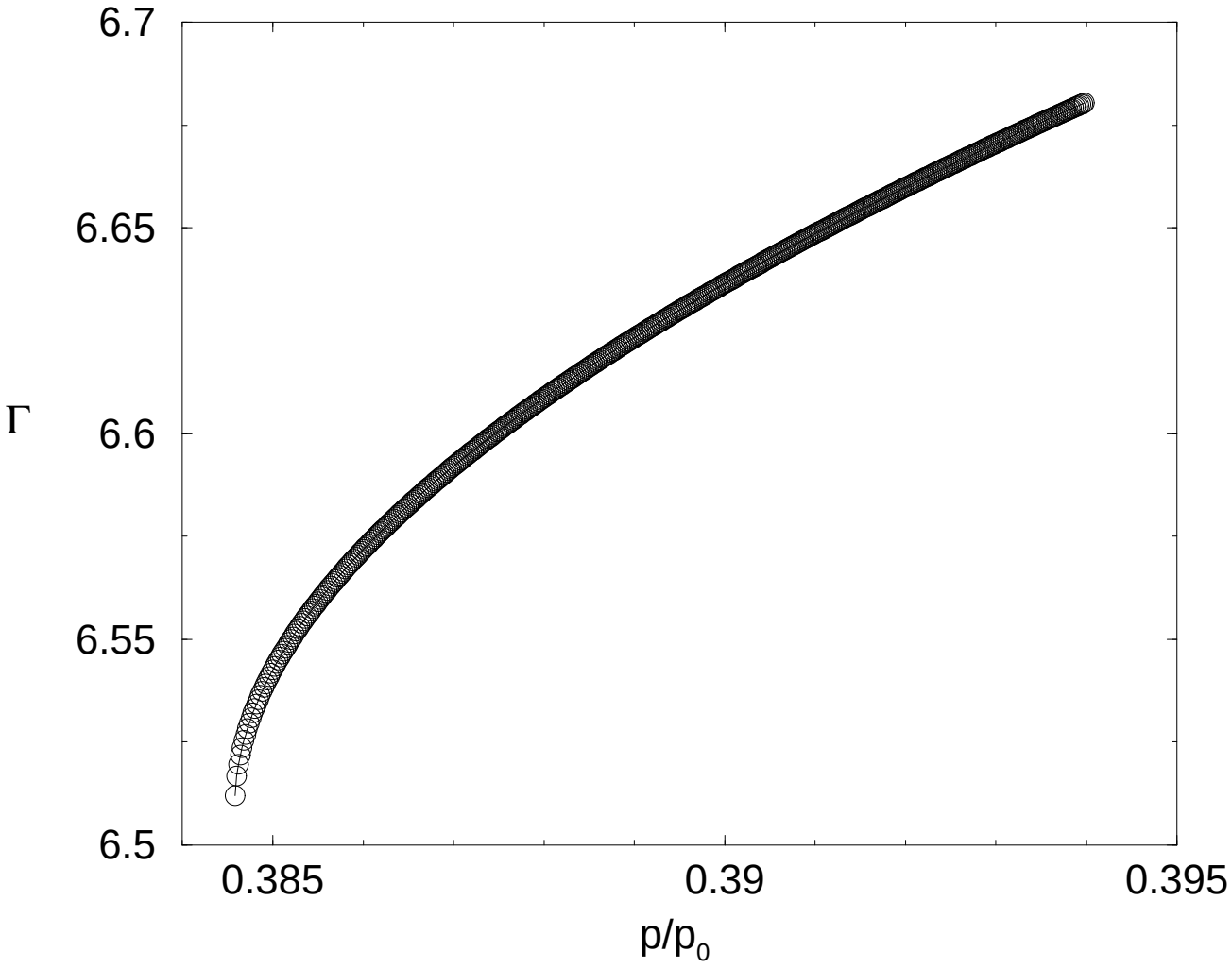

Figure 5: O. Gijzeman and R. van Roij

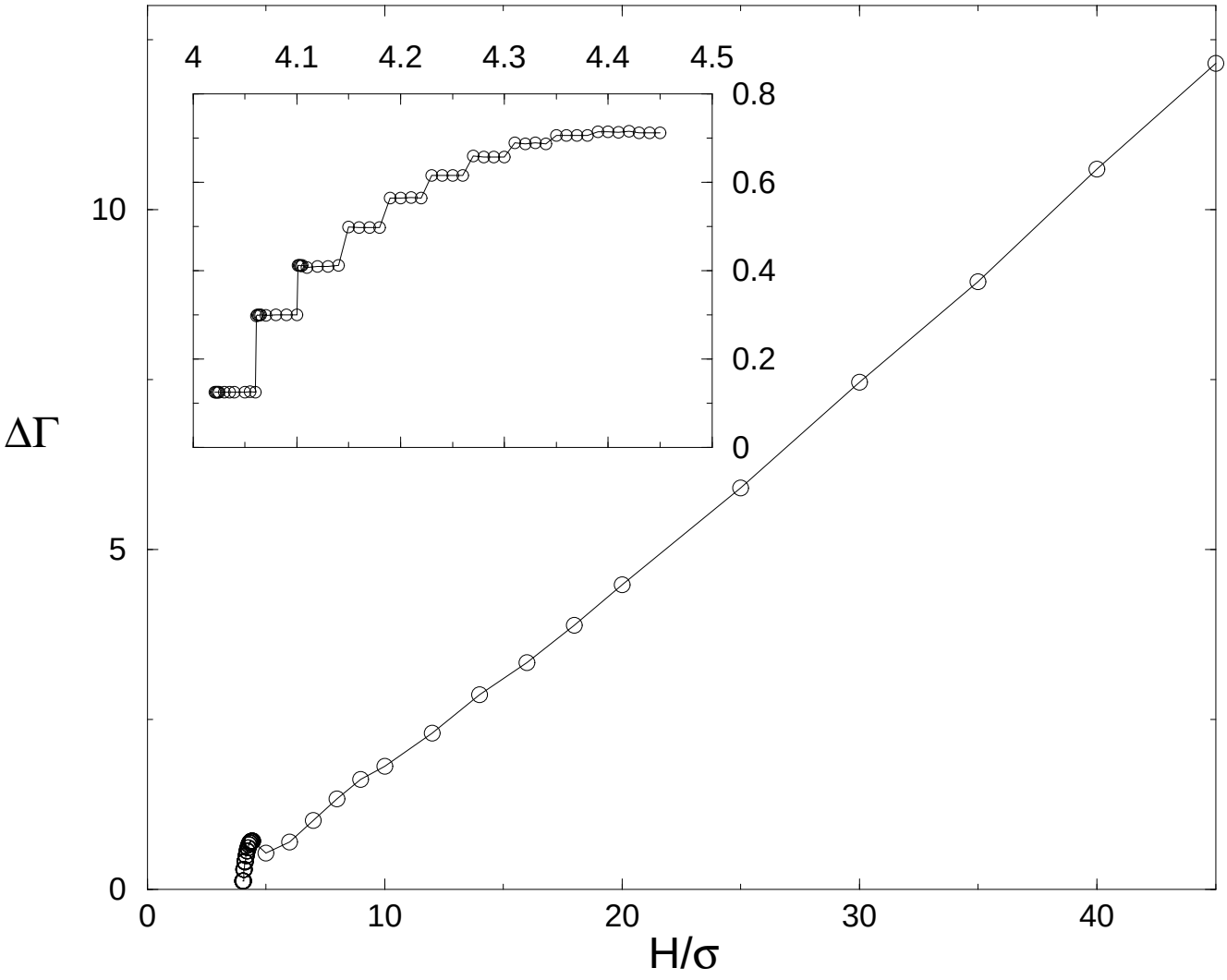

Figure 6: O. Gijzeman and R. van Roij

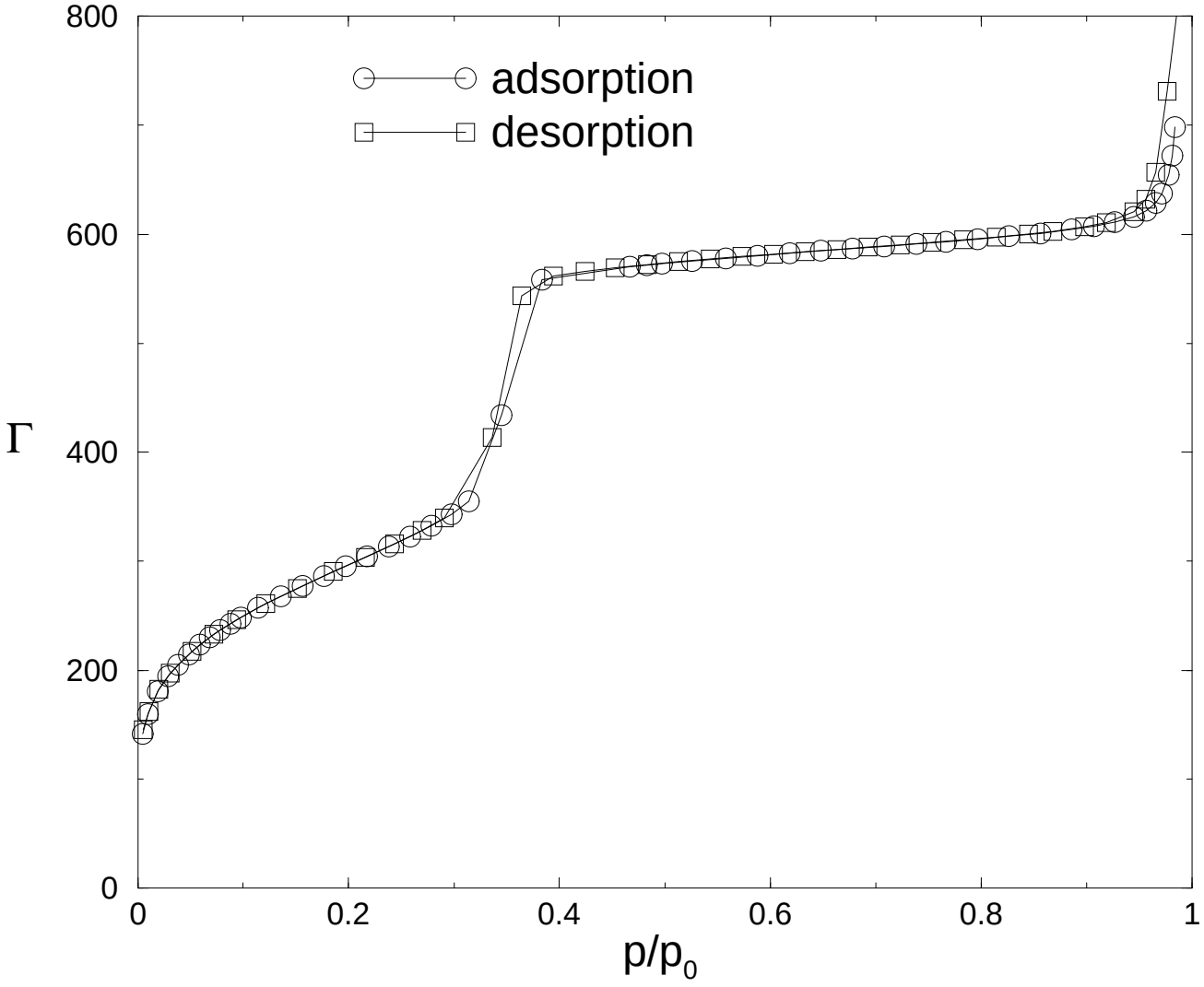

Figure 7: O. Gijzeman and R. van Roij

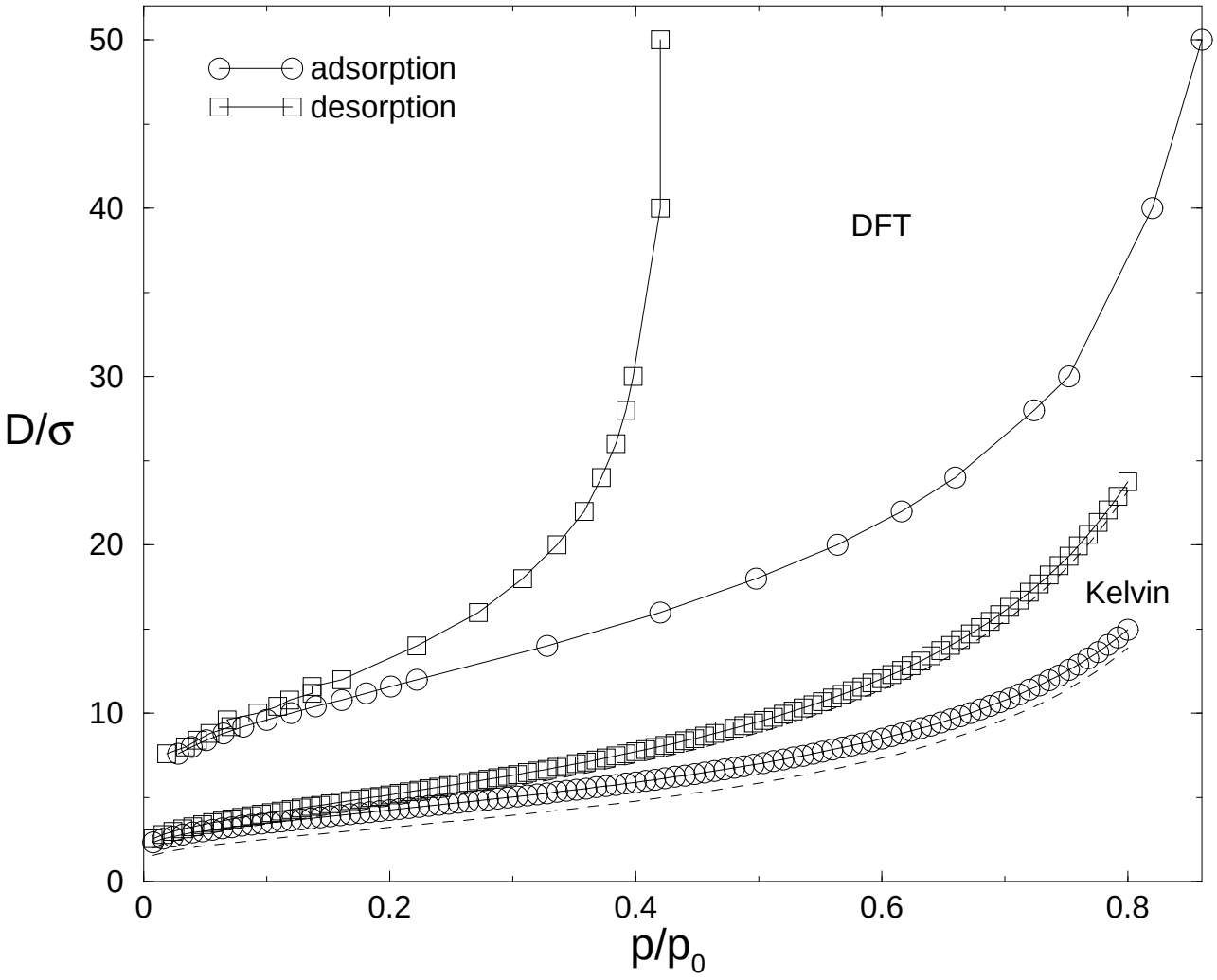

Figure 8: O. Gijzeman and R. van Roij

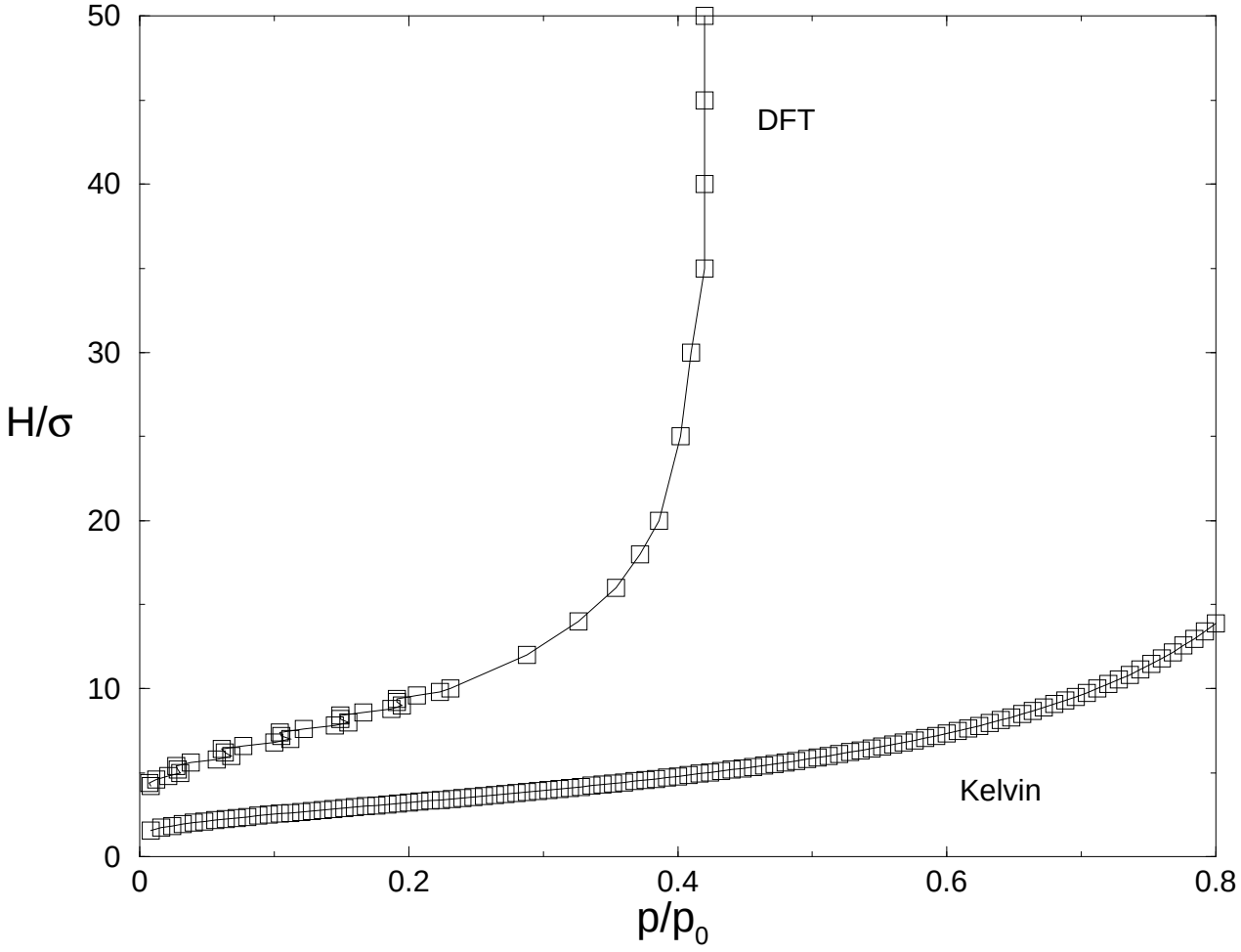

Figure 9: O. Gijzeman and R. van Roij

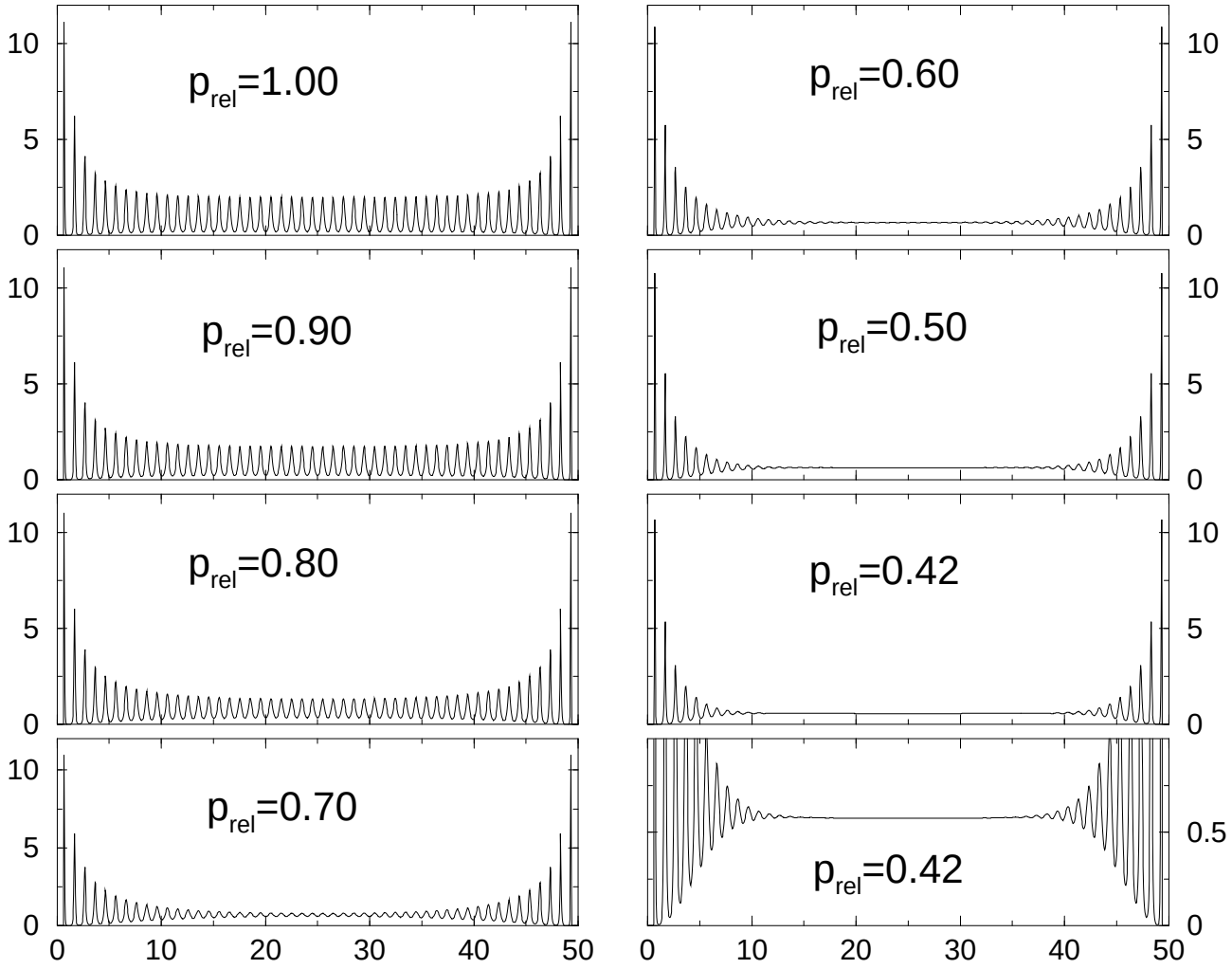

Figure 10: O. Gijzeman and R. van Roij